Interaction between Water Molecules and Zinc Sulfide Nanoparticles Studied by Temperature-Programmed Desorption and Molecular Dynamics Simulations

Hengzhong Zhang,*,† James R. Rustad,‡ and Jillian F. Banfield†

Department of Earth and Planetary Science, University of California, Berkeley, 307 McCone Hall, Berkeley, California 94720, and Department of Geology, University of California, Davis, One Shields Avenue, Davis, California 95616

Received: December 22, 2006; In Final Form: February 14, 2007

We have investigated the bonding of water molecules to the surfaces of ZnS nanoparticles (~2−3 nm sphalerite) using temperature-programmed desorption (TPD). The activation energy for water desorption was derived as a function of the surface coverage through kinetic modeling of the experimental TPD curves. The binding energy of water equals the activation energy of desorption if it is assumed that the activation energy for adsorption is nearly zero. Molecular dynamics (MD) simulations of water adsorption on 3 and 5 nm sphalerite nanoparticles provided insights into the adsorption process and water binding at the atomic level. Water binds with the ZnS nanoparticle surface mainly via formation of Zn−O bonds. As compared with bulk ZnS crystals, ZnS nanoparticles can adsorb more water molecules per unit surface area due to the greatly increased curvature, which increases the distance between adjacent adsorbed molecules. Results from both TPD and MD show that the water binding energy increases with decreasing the water surface coverage. We attribute the increase in binding energy with decreasing surface water coverage to the increasing degree of surface under-coordination as removal of water molecules proceeds. MD also suggests that the water binding energy increases with decreasing particle size due to the further distance and hence lower interaction between adsorbed water molecules on highly curved smaller particle surfaces. Results also show that the binding energy, and thus the strength of interaction of water, is highest in isolated nanoparticles, lower in nanoparticle aggregates, and lowest in bulk crystals. Given that water binding is driven by surface energy reduction, we attribute the decreased binding energy for aggregated as compared to isolated particles to the decrease in surface energy that occurs as the result of inter-particle interactions.

1. Introduction

There are increasing concerns about the risks of exposing/disposing of engineered nanoparticles to the environment and the safety of their applications in human-related products such as medication, cosmetics, and fabrics.[1,2] Studies show that nanoparticles may deposit in the human respiratory tract with quite high probability.[3] ZnO nanoparticles can damage *Escherichia coli* cells[4,5] and may be dangerous to human cells. To assess the previous concerns scientifically, it is necessary to investigate the nature of the nanoparticle−environment interactions. This includes how molecules are adsorbed by nanoparticles, the binding strength between them, and the changes in structure and reactivity induced by the interaction.

Water is ubiquitous in our environment and exists in all biological entities. Thus, the study of nanoparticle−water interactions serves as an important first step in understanding nanoparticle−environment interactions. Li et al. studied the interaction of water and carbon nanoparticles using molecular dynamics (MD) simulations.[6] They found that there is a strong water−surface interaction due to the high density of surface atoms in nanoparticles as compared to the bulk material. Redfern et al. studied catechol and water interactions with titanium oxide nanoparticles using ab initio molecular orbital theory and density functional theory.[7] Their results show that molecular adsorption of water on the (101) anatase surface is more favorable than dissociative adsorption. In our previous studies, we discovered that the adsorption of water molecules on small ZnS nanoparticles causes structure changes in the nanoparticles.[8,9] The interaction strength is yet to be determined, and the atomic details have not been elucidated. In the present work, we used temperature-programmed desorption (TPD) to determine the bonding strength between water molecules and ZnS nanoparticles and provide insights into their interactions at the atomic level via MD simulations.

2. Experimental Procedures

2.1. Sample Preparation. A total of 0.03 mol of $ZnCl_2$ (Fisher Chemical) and 0.03 mol of $Na_2S{\cdot}9H_2O$ (Mallinckrodt, Inc.) were dissolved in 200 mL of deionized (D.I.) water in two beakers, respectively. Then, the Na_2S solution was dripped into the $ZnCl_2$ solution slowly under magnetic stirring, forming white ZnS precipitates gradually. The reaction was complete after ~1.5 h. The precipitates were separated from the solution using gravity filtration. D.I. water was used to wash the precipitates during the filtration until the pH of the filtrate was close to 7. The precipitate was dried at 80 °C in air and then kept in vials for further use. This air-dried ZnS sample still contained ~14% water moisture.

2.2. X-ray Diffraction (XRD). A total of 10−30 mg of ZnS precipitates was dispersed in ~0.5 mL of acetone and then

* Corresponding author. Tel.: (510) 643-9120. E-mail: heng@eps.berkeley.edu.
† University of California, Berkeley.
‡ University of California, Davis.

10.1021/jp0688916 CCC: $37.00
Published on Web 05/23/2007

dripped onto a low-background silica plate using a pipet. A thin layer of fine ZnS powders was formed on the surface of the plate after evaporation of the acetone. The plate was loaded into the sample holder of a X-ray diffractometer (PANalytical X'Pert PRO) for XRD analysis. In the XRD determination, the diffractometer was operated at 40 kV and 40 mA with a Co Kα radiation X-ray source (X-ray wavelength 1.7903 Å). XRD patterns were collected in the 2θ range of 20−90° with a scanning rate of ∼1°/min.

2.3. Specific Surface Area. An accelerated surface area and porosimetry system (Micrometrics ASAP 2010) was used for surface area determination. A desorption tube loaded with ∼30 mg of the ZnS sample was mounted into the desorption chamber of the apparatus. The sample was heated to 400 °C and then held at that temperature for 2 h under continuous vacuum pumping to remove adsorbed water. The dried sample was then transferred under nitrogen atmosphere to the measurement chamber of the apparatus. The adsorption/desorption isotherms of nitrogen gas at 77 K on the sample were determined under computer control. The specific surface area of the sample was calculated using the Brunauer−Emmett−Teller equation (the so-called BET method). The phase of the sample after BET determination was reexamined by XRD.

2.4. TPD. The desorption function of the surface area and porosimetry system was used to conduct TPD of water from nanoZnS samples and a bulk ZnS sample that was obtained by hydrothermal coarsening of nanoZnS at 250 °C for 3 days. A ZnS sample of ∼50−130 mg was put into a desorption tube, and then the tube was connected to the desorption chamber of the apparatus and held at 50 °C for ∼2 h under continuous vacuum pumping (at ∼1 μmHg, i.e., 0.001 Torr pressure) to remove physically adsorbed water molecules from the sample. Then, the sample temperature was ramped linearly with time to 450 °C at ∼7−12 °C/min. Water molecules desorbed continuously as the temperature increased, and the pressure in the chamber varied with the time as TPD proceeded. The pressure and temperature display from the apparatus were recorded using a webcam. The saved video files were later replayed and read into ($P-T-t$) numerical values for data processing.

3. Molecular Dynamics Simulations

3.1. Interatomic Potential Functions. In the literature, several sets of interatomic potential functions have been employed to conduct MD simulations of ZnS crystals.[10−12] In the present work, we adopted the shell model[13] of ZnS by Wright and Jackson,[10] which is compatible with the MD simulation code DL_Poly[14] employed in this work, although a more complicated set of interatomic potential functions was derived by the same group recently.[15] With the potential set of ref 10, each Zn (or S) atom was modeled as a core and a shell connected via a spring, accounting for the ionic polarity of the atoms induced under a local electric field. The cores of Zn and S atoms are neutral, but each shell carries a charge of +2 and −2, respectively. The short-range non-Coulombic interaction between two atoms i and j takes the Buckingham form of

$$u_{ij}\,(\text{short-range}) = A_{ij}\exp\left(-\frac{R_{ij}}{\rho_{ij}}\right) - \frac{C_{ij}}{R_{ij}^{\,6}} \qquad (1)$$

where u_{ij} is the interaction potential, R_{ij} is the distance between atoms i and j, and A_{ij}, ρ_{ij}, and C_{ij} are the three model parameters. An angle-bending form of three-body interactions is considered for the nearest S−Zn−S atoms

$$u_{ijk} = \frac{1}{2}k_{ijk}(\theta - \theta_{ijk})^2 \qquad (2)$$

where u_{ijk} is the interaction potential, k_{ijk} is a model parameter, θ is the angle formed by atoms i (S), j (Zn, center), and k (S), and θ_{ijk} is the equilibrium value of the angle (109.4°). For detailed values of the model parameters, please refer to ref 10.

Following previous work,[9] we have chosen the shell water model of De Leeuw[16] for the MD simulations of the ZnS−H_2O interactions. With the shell water model, O carries a charge of −0.8 (core 1.25 and shell −2.05), and H carries a charge of 0.4 (core only). The OH bond in the water molecule was modeled using a Morse potential; a bond-bending equation (eq 2) was used in modeling the H−O−H angle. Atomic interactions between O shells and between H cores and O shells are described by the Lennard-Jones equation and the Buckingham equation, respectively. For a detailed description of the shell water model, see ref 16.

In our previous work,[8,9] the Zn−H and S−O interactions were assumed to be purely electrostatic. In addition to the electrostatic interactions, the short-range non-Coulombic interaction for Zn−O was taken from ref 17 in the Buckingham form and that for S−H was obtained by fitting the Buckingham equation to the ground state potential energy surfaces of H_2S gas calculated from first principles analysis.[18] Phase stability and structure change of ZnS nanoparticles upon water adsorption were correctly predicted by MD with these potential functions.[8,9] However, since the S−H interaction was derived from the pure gas-phase H_2S data, the interaction strength may be overestimated. Thus, in the present work, we decided to fit new potential functions for the S−H and S−O pairs with available water binding energy of one H_2O molecule on bulk ZnS[19] and the H_2O−H_2S interactions calculated from first principles analysis.[20]

3.2. Molecular Dynamics Simulations. 3.2.1. MD of a Zn−S Cluster in Water. To test and validate the newly derived ZnS−H_2O potential sets, both classical MD and Car−Parrinello MD (CPMD) simulations[21] were performed for a Zn_4−S_4 cluster immersed in water (59 H_2O molecules) at periodic boundary conditions and in a canonical assemble (constant NVT) at 300 K. The CPMD calculations were carried out with NWChem,[22] employing a plane-wave basis (energy cutoff = 90 AU) with Troullier−Martins pseudo-potentials[23] and the PBE96 exchange-correlation functional.[24] We used Car−Parrinello dynamics with the fictitious mass set at 400 AU. Electronic and nuclear degrees of freedom were attached to separate Nose−Hoover thermostats having masses of 250 AU.[25] The snapshot of the atomic configuration taken from the CPMD was used as the initial setup for the classical MD. The classical MD was conducted for a MD time period of 100 ps with a time step of 0.1 fs. The configurations sampled from both classical MD and CPMD were examined and compared with each other.

3.2.2. MD of ZnS Nanoparticles. Initial configurations of 3 and 5 nm ZnS nanoparticles were constructed from atomic coordinates of bulk sphalerite ZnS. They contain 360 and 1061 ZnS molecular units, respectively. The MD simulations of the 3 and 5 nm ZnS nanoparticles were run for 50 and 25 ps, respectively, with a time step of 0.5 fs in the canonical assemble at 300 K using the Nose−Noover thermostat. At these time scales, both structures were fully relaxed as indicated by the rapid decreases in the potential energy at the beginning of the MD runs and the minor fluctuations of the energy around constant values after ∼2 ps in the simulations.

3.2.3. MD of H_2O Gas Molecules. Water molecules (1, 19, 86, and 228 H_2O) were randomly put into cubic boxes big enough to simulate water vapor rather than liquid water (each

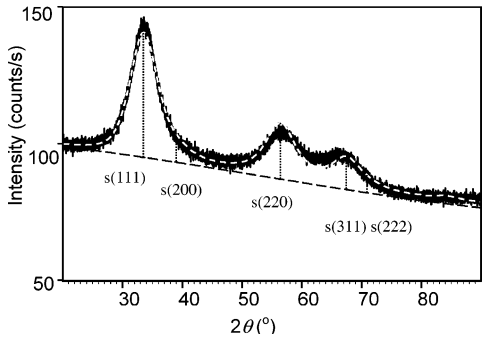

Figure 1. XRD pattern of synthesized nanocrystalline ZnS (thick black curve). Rietveld analysis (dashed white curve) shows that ZnS is in the sphalerite phase, as shown by the indexed reflection peaks.

side was 100−400 Å). The MD simulations were run at periodic boundary conditions and in canonical assemblies at 300 K for 50 ps with a time step of 0.5 fs. Gas water molecules formed in the big simulation boxes. The average potential energy of each gas water molecule can be calculated from these simulations and will be used in the calculations of binding energies of gas water molecules on ZnS nanoparticles.

3.2.4. MD of Adsorption of H_2O Molecules on ZnS Nanoparticles. Initial configurations of the 3 and 5 nm ZnS nanoparticles were obtained from the output of previous MD simulations of individual ZnS nanoparticles. A thin spherical shell of water molecules was cut from equilibrated bulk water coordinates and placed over the surface of the ZnS nanoparticle. For simulations of water adsorption on the 3 nm ZnS particle, MD runs were conducted with the following 19 different numbers of water molecules: 8, 15, 43, 58, 69, 82, 95, 104, 111, 121, 141, 153, 161, 172, 188, 234, 263, 297, and 362. For the 5 nm ZnS particle, eight different numbers of water molecules were employed: 108, 163, 252, 441, 623, 742, 931, and 1115. Each MD simulation was performed in a canonical assembly at 300 K with a time step of 0.5 fs for about 50 ps for the case of 3 nm ZnS + H_2O and for 5−8 ps for the case of 5 nm ZnS + H_2O. A shorter MD time was used for the latter case because of the large number of atoms in the system. In both the 3 and the 5 nm cases, the potential energy of a simulation reached a steady value in the MD. Adsorption of water molecules on the ZnS nanoparticle readily can be seen from the trajectory analyses of the MD outputs.

4. Results and Discussion

4.1. Sample Characterization. The XRD pattern (Figure 1) of the synthesized ZnS sample was collected for phase identification and particle size calculation. The XRD pattern shows broadened diffraction peaks of the sphalerite phase, marked by the three strong reflections from the (111), (220), and (311) lattice planes. Rietveld fitting was used to further confirm the sphalerite phase, as evidenced by the fact that the fitted profile coincides with the experimental one very well (Figure 1). From the Rietveld analysis, the average particle size of ZnS was calculated to be 2.0 nm based on the broadening of the XRD peaks. Transmission electron microscopy (TEM) observation of the sample from our previous work[26] showed that most ZnS nanoparticles are close to spherical and are in the size range of 2−3 nm, consistent with the XRD size estimation.

The specific surface area of the sample was determined to be 56.2 m^2/g of ZnS using the BET method. This corresponds to an average grain size of 26 nm assuming that all grains are spherical. Thus, the synthesized ZnS nanoparticles existed in aggregated forms, with each grain consisting of around 1000 primary ZnS nanoparticles on average. (Approximately, the primary particle number equals the volume ratio V(grain)/V(primary particle) = $(26/2.5)^3 = 1000$.) After the BET determination, the sample was reexamined by XRD, which showed that ZnS was still in the sphalerite phase with an average particle size of 2.5 nm. There was no significant coarsening during the BET determination.

4.2. TPD Kinetics. The kinetics of a TPD process can be described by the Polanyi−Wigner equation[27,28]

$$-\frac{d\theta}{dt} = \nu_d \theta^n \exp\left(-\frac{E_d}{RT}\right) \tag{3}$$

where θ is the surface coverage of the adsorbate (water molecules), T is the absolute temperature, R is the gas constant (8.314 J/mol K), and n, ν_d, and E_d are the reaction order, pre-exponent factor (frequency factor), and activation energy, respectively, for the desorption reaction. The three kinetic parameters n, ν_d, and E_d may be functions of the surface coverage θ. In a TPD system, when the pumping rate is relatively high in reference to the sample mass and the heating rate, the pressure P (above the background) is proportional to the desorption rate ($-d\theta/dt$).[27] In this case, eq 3 can be written as

$$P = K\nu_d \theta^n \exp\left(-\frac{E_d}{RT}\right) \tag{4}$$

where K is a proportional constant. In general, the unknown kinetic parameters are determined through numerical fitting of the pressure profile.

In the experiments, ZnS samples were pre-desorbed at 50 °C at a high vacuum so that most physically adsorbed multilayer water molecules (∼10% wt) were removed before a TPD measurement. After a TPD measurement, the sample further lost ∼4% in weight. Thus, at the beginning of a TPD measurement ($t = 0$), the surface coverage of water molecules is

$$0.04 \times 6.023 \times 10^{23}/18.02\ H_2O/(56.2 \times 10^{18}\ nm^2\ ZnS) \approx 24\ H_2O/nm^2\ ZnS$$

(The surface area of the 3 nm ZnS sample is 56.2 m^2/g.) At this surface coverage, all chemical binding sites for water molecules on the ZnS nanoparticle surfaces can be considered fully occupied. Hence, the surface coverage θ can be regarded as 1 at $t = 0$.

Figure 2a shows typical TPD curves for water desorption from the synthesized 3 nm ZnS sample. The pressure quickly reached a maximum value after ∼15 min, then decreased and approached the background at ∼1 h. To model the TPD kinetic curves, we made the following assumptions. First, water molecules are molecularly absorbed on ZnS surfaces, hence the desorption reaction order $n = 1$. Second, the pre-exponent factor (ν_d) is independent of the surface coverage θ and the temperature T. A general polynomial form is used to describe the variation of the activation energy with the surface coverage

$$E_d = a_0 + \sum_{i=1}^{3} a_i \theta^i \tag{5}$$

where a_0−a_3 are coefficients to be determined.

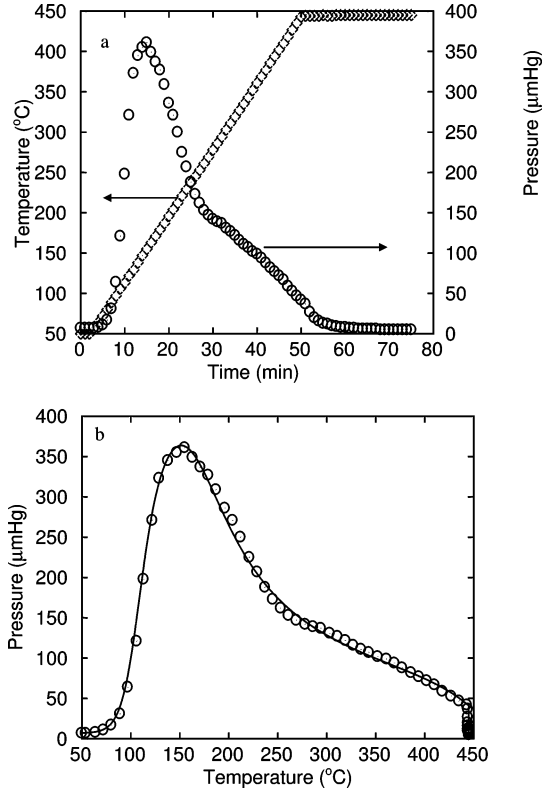

Figure 2. (a) TPD curves for a 2−3 nm ZnS sample and (b) kinetic modeling of the pressure profile. Experimental data are shown in points and kinetic modeling in a solid curve (b).

We used the following procedure to obtain the unknown kinetic parameters ($K\upsilon_d$) and a_0 to a_3. First, we generated a few thousand data points through interpolation of the recorded $t-T-P$ data points (see Figure 1a) at a time interval of 0.02 min. Such a small time step was required for a numerical solution of eq 3. The interpolated $t-T-P$ data then were loaded into a spreadsheet (MS Excel) for numerical solution of eq 3. Since the parameters a_0-a_3 for E_d (eq 5) and υ_d and K in eqs 3 and 4 were unknown, they were given estimated values. Then, we solved eq 3 numerically using a simple Euler method at the initial condition of $t = 0$, $\theta = 1$, and $T = 323$ K (50 °C). The pressure was calculated using eq 4 at every time step for the integration of eq 3. Then, the square of the difference between the calculated pressure and the measured value (from interpolation) at each time step (i) was summed over the whole time range

$$s = \sum_i (P_{\text{calculated}} - P_{\text{measured}})^2 = f(K\upsilon_d, a_0 ... a_3) \qquad (6)$$

By minimization of the quantity s through optimized adjustment of the unknown parameters, $K\upsilon_d$ and $a_0 ... a_3$ were derived. Figure 2b shows that the calculated pressures (eq 4) through the previous kinetic modeling well-reproduced the measured values. For a series of TPD measurements at different heating rates (7.4−12.3 °C/min), the derived parameters are summarized in Table 1.

A previous study[29] showed that the activation energy of water desorption from rutile is close to the heat of adsorption of water, meaning that the activation energy for adsorption is low when compared to that for desorption. Thus, in the present work, we regard the activation energy for desorption of water as the binding energy of water molecules on the 3 nm ZnS nanoparticles. Figure 3 shows that the binding energy of water molecules decreases with increasing surface coverage, as calculated from eq 5 using the coefficients in Table 1. A similar trend was also observed in water bonding on nanometer-sized γ-alumina.[30] Such a phenomenon is explained next.

4.3. Derivation of S−H and S−O Interaction Functions for MD. Les[20] calculated the intermolecular potential energies for the systems H_2O-H_2S, H_2O-H_2Se, and H_2S-H_2S with pseudo-potentials using optimized basis sets. The H_2S-H_2O intermolecular potential energy is a function of their separation distance (Figure 2 of ref 20). The energies were corrected to include dispersion (ref 20). Using density functional theory method, Steel et al.[19] calculated the binding energy of one water molecule on the (110) surface of bulk ZnS (sphalerite) in two configurations (Figure 5 of ref 19). The corrected H_2S-H_2O intermolecular potential energies[20] and the water binding energies on the ZnS (110) surface[19] were used for our derivation of the S−H and S−O interatomic potential functions using the program GULP.[31] In the optimization, we assumed the Buckingham form for the S−H and S−O interactions (eq 1), the Zn−O interaction was from ref 17, and both ZnS and water were described by their respective shell models.[10,16] The optimized Buckingham parameters are listed in Table 2. The optimized potential well-reproduced the intermolecular potential energies of the H_2S-H_2O system and reasonably reproduced the binding energies of one H_2O on the ZnS (110) surface (Table 3). In the optimization, the program may have biased the data from ref 20 because it contributed more data sets than ref 19.

The validity of the newly derived S−O and S−H potential functions for the description of the water−ZnS interaction was tested by comparison of the results from classic MD and CPMD for a Zn_4-S_4 cluster in 59 H_2O (300 K in periodic conditions). Figure 4 illustrates snapshots of the cluster bound by water molecules. In both MD and CPMD, a Zn_3-S_3 ring formed. One, two, or three water molecules bound with the Zn_4-S_4 cluster mainly via bonding of the water oxygen atoms with the Zn atoms in the cluster. Figure 5 shows calculated radial distribution functions (RDF) of different atomic pairs from the two snapshots. It is seen that the RDFs calculated from the MD output are quite consistent with those calculated from the CPMD output.

4.4. Perspective of Water Binding on ZnS Nanoparticles by MD. There are possibly three ways for water molecules to bind with ZnS nanoparticle surfaces: (a) via formation of Zn−O bonds; (b) via formation of S−H bonds; and (c) via formation of both Zn−O and S−H bonds. MD simulations show that case a is the predominant process, as seen from Figure 6, also seen from Figure 4, although case b also exists. In the MD/CPMD of the Zn_4-S_4 cluster (Figure 5), the shortest Zn−O distance is ∼2.0 Å, while that for S−H is ∼2.3 Å, suggesting that the Zn−O bond is stronger than the S−H bond. This can be understood simply by considering that the difference between the Pauling electronegativities[32] of O and Zn (3.44−1.65 = 1.79) is larger than that between S and H (2.58−2.20 = 0.38). Thus, water molecules interact with ZnS nanoparticle surfaces mainly via the formation of Zn−O bonds.

Figure 6 shows a snapshot of a 3 nm ZnS particle after adsorption of 362 H_2O molecules. Detailed analysis of this structure showed that a surface Zn site can adsorb one to four H_2O molecules, depending on the local structure of the Zn site. Usually, the more open the Zn site (e.g., a Zn site at the outermost surface layer of the nanoparticle), the higher the number of bound water molecules. In addition, some water molecules can also bond with the ZnS surface via S−H interactions. Thus, it is expected that the maximum surface

TABLE 1: Kinetic Parameters for Water Desorption from 3 nm ZnS (Sphalerite) Nanoparticle Aggregates

heating rate (K/min)	sample mass (mg)	a_0 (kJ/mol)	a_1 (kJ/mol)	a_2 (kJ/mol)	a_3 (kJ/mol)	$K\nu_d$ ($\times 10^{20}$ μHg/mg)
7.4	49.4	222.14	−242.19	243.78	−97.06	0.54
8.2	126.5	226.22	−231.32	223.71	−91.78	0.57
9.3	65.0	221.23	−238.53	244.74	−100.54	0.48
9.5	51.8	221.15	−234.67	240.62	−98.94	0.41
12.3	53.1	226.94	−223.18	211.78	−81.16	0.42
mean values		223.53 (2.81)[a]	−233.98 (7.29)	232.93 (14.56)	−93.90 (7.83)	0.48 (0.07)

[a] Data in parentheses are the standard deviations.

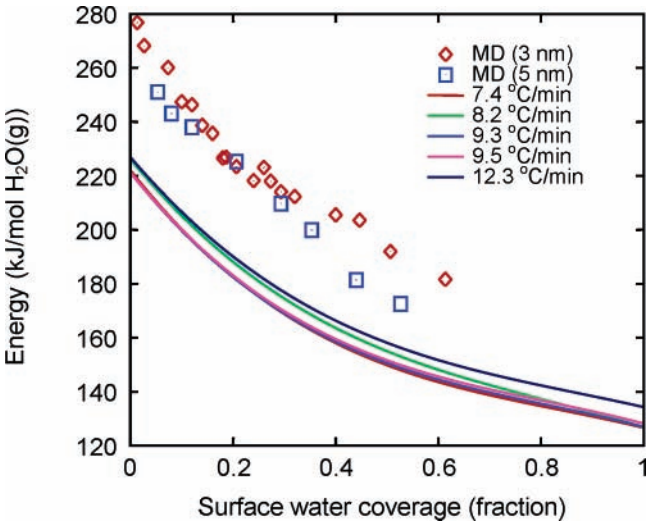

Figure 3. Binding energy of water on ZnS nanoparticles. Solid lines are for aggregated ZnS nanoparticles derived from kinetic modeling of the TPD curves measured at different heating rates (7.4−12.3 °C/min). Points are from estimations by MD of isolated (i.e., non-aggregated) ZnS nanoparticles.

TABLE 2: Interatomic Interaction Potential Parameters (Eq 1)

atomic pair	A (eV)	ρ (Å)	C (eV Å^6)
S−H	41399.49	0.2039	0
S−O	4268.15	0.3686	965.33

TABLE 3: Comparison between Literature and Calculated Energy Data

Intermolecular potential energy between H_2S and H_2O

distance (S−O) (Å)	energy (corrected)[20] (kJ/mol)	energy (calcd) (kJ/mol)
2.91	13.96	14.03
3.17	−7.38	−7.33
3.44	−13.31	−13.40
3.70	−13.34	−13.30
3.97	−11.49	−11.56

Binding energy of one H_2O on ZnS (110) surface

Configuration	energy[19] (kJ/mol of H_2O)	energy (calcd) (kJ/mol of H_2O)
1	74.48	54.14
2	19.25	23.01

coverage of water in ZnS nanoparticles is much higher than that in bulk ZnS crystals. This was confirmed by a TPD experiment of bulk ZnS. In the TPD experiment of bulk ZnS, it was observed that after pre-desorption at 50 °C, there was no pressure increase during a temperature ramping to 450 °C. This indicates that there was no detectable chemically absorbed water in the bulk material after pre-desorption.

From MD, there are ~200 Zn and 200 S surface sites on the 3 nm ZnS nanoparticle surface. Assuming that on average each

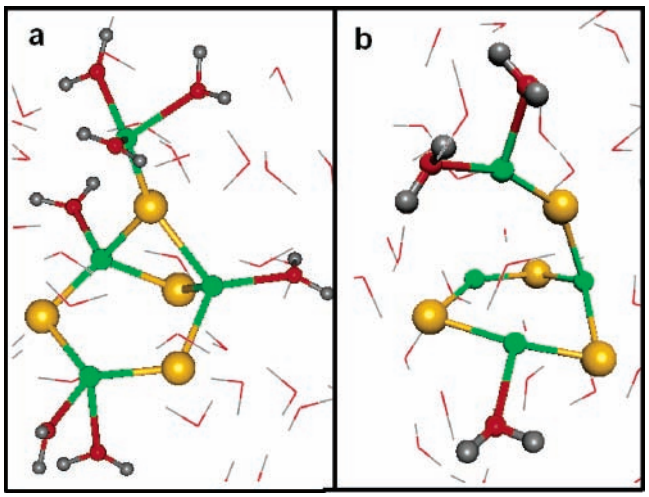

Figure 4. Snapshots of a Zn_4-S_4 cluster in water (59 H_2O) from (a) MD and (b) CPMD. Periodic boundary conditions were employed in both MD and CPMD simulations. Water molecules not bound by the cluster via Zn−O bonding are rendered in lines. Zn: green; S: yellow; O: red; and H: gray.

Zn site can adsorb 2.5 H_2O molecules and each S site can adsorb 0.5 H_2O molecules, then the maximum number of chemically adsorbed water molecules on the nanoparticle is 3.0×200 $H_2O/\pi 3^2$ nm^2 $\approx$ 21 H_2O/nm^2. This value coincides with the initial water surface coverage estimated from the TPD weight loss (24 H_2O/nm^2). Thus, the surface coverage θ can be considered to be one at the beginning of a TPD (at $t = 0$).

The binding energy of water on ZnS nanoparticles can be calculated from the potential energy difference of various equilibrated MD systems

$$E(\text{binding energy}) = -\frac{E_{pot}(ZnS + H_2O) - E_{pot}(ZnS) - n_{water}E_{pot}(H_2O)}{n_{water}} \quad (7)$$

where $E_{pot}(ZnS + H_2O)$ or $E_{pot}(ZnS)$ is the potential energy of a ZnS nanoparticle with or without water adsorption, $E_{pot}(H_2O)$ is the potential energy of 1 mol of gas H_2O molecules, and n_{water} is the molar number of water molecules adsorbed by the ZnS nanoparticle. All quantities in the equation were obtained from the MD simulations by averaging the potential energy at the MD equilibration stage (for all cases, potential energy fluctuations were less than 1 kJ/mol). Figure 3 shows the calculated binding energies of water on 3 and 5 nm ZnS nanoparticles.

Figure 3 shows that the binding energy of water molecules (as given by both TPD and MD) decreases with increasing surface coverage. At a higher surface coverage, more nanoparticle surface sites are coordinated by adsorbed water molecules; hence, there is a stronger intermolecular interaction between adsorbed water molecules. The hydrogen−oxygen bonding

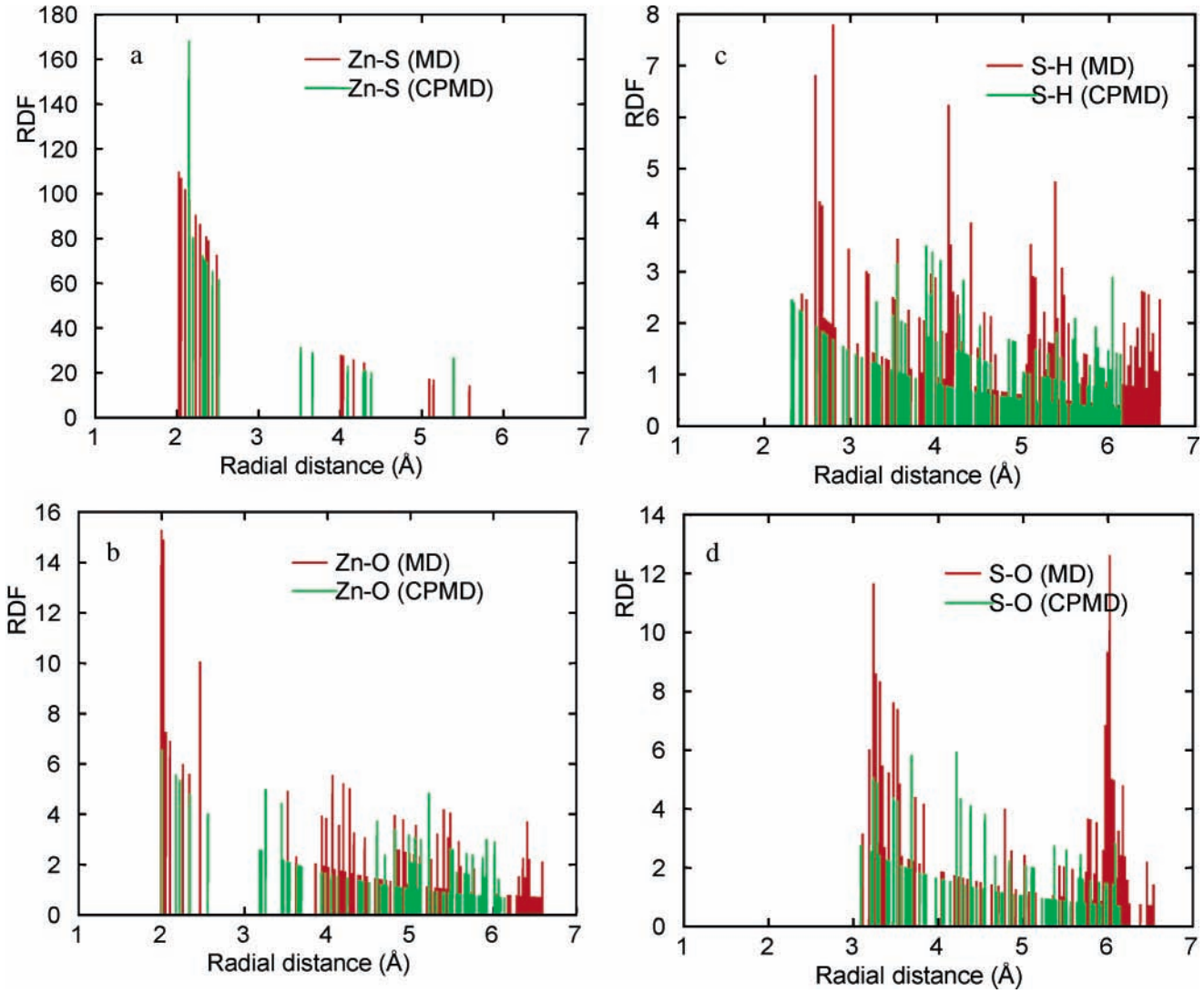

Figure 5. Atomic radial distribution functions (RDF) predicted by the MD (red lines) and CPMD (green lines). (a) S around Zn; (b) O around Zn; (c) H around S; and (d) O around S.

between adjacent water molecules partially shields the further interaction of O atoms in water molecules with the Zn atoms in the ZnS nanoparticles, as evidenced by the increased Zn−O bond length (calculated from MD structures) at a higher number of adsorbed water molecules (Table 4). As a result, the binding strength and thus the binding energy of water decrease with the increase of water surface coverage.

A size effect on the binding energy can be discerned: the bigger the nanoparticle, the lower the binding energy (Figure 3). A larger nanoparticle has a lower surface curvature. Thus, in a larger nanoparticle, the interaction between two adjacent adsorbed water molecules is stronger than in a smaller nanoparticle because they are closer together on a lower curvature surface. This reduces the water binding energy at larger particle sizes. It is also noted that the value of the slope ($|\Delta E/d\theta|$) at high water coverage is greater for the 5 nm particle than for the 3 nm particle. This is because there is a stronger interaction between adsorbed water molecules on the 5 nm particle, which lowers the energy of binding of water to the nanoparticle surface to a greater degree when the same amount of water molecules is added by adsorption. Previously, we found that organic compounds have a higher affinity on bonding with smaller titania nanoparticles.[33] This can be explained if we assume that an organic compound has a higher binding energy in smaller titania nanoparticles based on the present MD results.

As compared with the TPD derived water binding energy, the MD derived value (for the 3 nm ZnS) is about ∼30−60 kJ/mol higher than that from the former (Figure 3). However, they do show similar dependences on the surface coverage of water. The difference between the TPD and MD derived binding energies can be attributed to the difference between the aggregation states of ZnS. In the MD, the simulated ZnS were isolated individual nanoparticles (3 or 5 nm), while in the TPD, the nanoparticles were highly aggregated ZnS (each contained ∼1000 3 nm primary particles). The aggregation effectively reduced the surface energy of the agglomerated primary particles via inter-nanoparticle interactions. In turn, the lowered surface energy makes the water−nanoparticle interaction weaker. Thus, the water binding energy for aggregated nanoparticles (as determined by the TPD experiments) is lower than that for the isolated nanoparticles (as given by the MD).

Values of water binding energy on bulk ZnS are available from a previous study on water adsorption/desorption in bulk ZnS by Sagaguchi and Shibuki.[34] Their results show that the water binding energy is ∼105 kJ/mol at the water surface coverage $\theta \rightarrow 0$ and is ∼38 kJ/mol at the water surface coverage $\theta \rightarrow 1$. Thus, the TPD derived water binding energy on 3 nm ZnS nanoparticles (Figure 3) is ∼90−120 kJ/mol higher than that on bulk ZnS crystals. Overall, the water binding energy

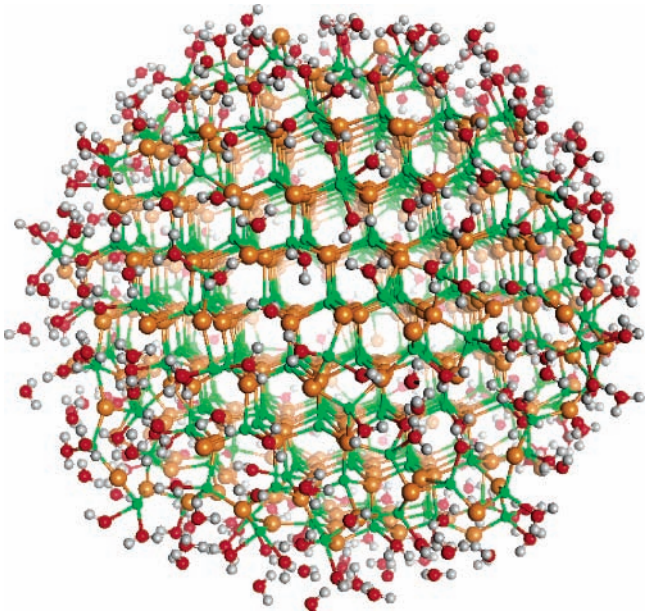

Figure 6. Snapshot of the structure of a 3 nm ZnS (sphalerite) particle after adsorption of 362 H_2O molecules in the MD. H_2O molecules interact with the nanoZnS surface mainly via formation of the Zn−O bonds and partially via formation of the S−H bonds. There are ~200 active Zn/S sites on the surface. Zn: green; S: orange; O: red; and H: gray.

TABLE 4: Calculated Average Lengths of Zn−O Bonds (Formed on H_2O−3 nm ZnS Interfaces) and Water Binding Energy Based on MD Results

no. of adsorbed H_2O molecules	av Zn−O bond length (Å)	binding energy (k/mol of H_2O)
8	1.944	276.8
104	1.955	226.6
153	1.959	223.1
263	1.971	203.5
362	1.988	181.6

increases in the sequence: bulk ZnS, ZnS nanoaggregates, and isolated ZnS nanoparticles.

4.5. Relevance to Environmental Safety of Nanoparticles. According to results from the present study, we infer the following. First, nanoparticles can accommodate more adsorbates per unit surface area than the corresponding bulk material because the surfaces of the former are more structurally open for coordination of absorbates. Second, adsorbates may bind with nanoparticles more strongly than with the corresponding bulk material because the binding energy for the former is higher than for the latter. These factors may be important for assessment of the environmental roles and impact of nanoparticles.

5. Conclusion

Through combined TPD and MD study, we identified two important consequences of water adsorption on ZnS particles as a result of the highly reduced particle size. First, ZnS nanoparticles can adsorb more water molecules per unit of surface area because of the significantly increased curvature and more open surface configuration. Second, the water binding energy is higher in nanoparticles than in bulk crystals (although compared with isolated nanoparticles, aggregation can reduce the binding energy) because the intermolecular interaction of water on the curved nanoparticle surfaces is not as strong as in flat bulk surfaces. Therefore, more water molecules can be adsorbed by ZnS nanoparticles at a stronger binding strength at the nanoparticle surfaces as compared to by bulk ZnS. This conclusion may be extended to other nanoparticles interacting with other molecules, such as environmental species. By extension, the current work presents an important scientific basis for the understanding of the environmental impact of engineered nanoparticles.

Acknowledgment. We thank Drs. W. Smith and J. D. Gale for providing MD programs DL_POLY and GULP. NWChem developed and distributed by PNNL was used to obtain some of the results. Financial support for this work was provided by the U.S. Department of Energy (Grant DE-FG03-01ER15218) and the National Science Foundation (Grant EAR-0123967).

References and Notes

(1) Gould, P. *Nanotoday* **2006**, *1*, 34.

(2) Dunphy-Guzman, K. A.; Taylor, M. R.; Banfield, J. F. *Environ. Sci. Technol.* **2006**, *40*, 1401.

(3) Maynard, A. D. *Nanotoday* **2006**, *1*, 22.

(4) Brayner, R.; Ferrari-Iliou, R.; Brivois, N.; Djediat, S.; Benedetti, M. F.; Fievet, F. *Nano Lett.* **2006**, *6*, 866.

(5) Gould, P. *Nanotoday* **2006**, *1*, 19.

(6) Li, L.; Bedrov, D.; Smith, G. D. *J. Phys. Chem. B* **2006**, *110*, 10509.

(7) Redfern, P. C.; Zapol, P.; Curtiss, L. A.; Rajh, T.; Thurnauer, M. C. *J. Phys. Chem. B* **2003**, *107*, 11419.

(8) Zhang, H.; Gilbert, B.; Huang, F.; Banfield, J. F. *Nature* **2003**, *424*, 1025.

(9) Zhang, H.; Huang, F.; Gilbert, B.; Banfield, J. F. *J. Phys. Chem. B* **2003**, *107*, 13051.

(10) Wright, K.; Jackson, A. *J. Mater. Chem.* **1995**, *5*, 2037.

(11) Hamad, S.; Cristol, S.; Catlow, C. R. A. *J. Phys. Chem. B* **2002**, *106*, 11002.

(12) Benkabou, F.; Aourag, H.; Certier, M. *Mater. Chem. Phys.* **2000**, *66*, 10.

(13) Dick, B. G.; Overhauser, A. W. *Phys. Rev.* **1958**, *112*, 90.

(14) Smith, S.; Forester, T. R. *The DL_Poly2 User Manual*, version 2.13; Daresbury Laboratory: Daresbury, Warrington, U.K., 2001.

(15) Wright, K.; Gale, J. D. *Phys. Rev. B* **2004**, *70*, 35211.

(16) De Leeuw, N. H.; Parker, S. C. *Phys. Rev. B* **1998**, *58*, 13901.

(17) Harris, D. J.; Brodholt, J. P.; Harding, J. H.; Sherman, D. M. *Mol. Phys.* **2001**, *99*, 825.

(18) Stevens, J. E.; Chaudhuri, R. K.; Freed, K. F. J. *Chem. Phys.* **1996**, *105*, 8754.

(19) Steele, H. M.; Wright, K.; Hillier, I. H. *Phys. Chem. Miner.* **2003**, *30*, 69.

(20) Les, A. *Theor. Chim. Acta* **1985**, *66*, 375.

(21) Car, R.; Parrinello, M. *Phys. Rev. Lett.* **1985**, *55*, 2471.

(22) Apra, E. et al. *NWChem, A Computational Chemistry Package for Parallel Computers*, version 4.7; Pacific Northwest National Laboratory: Richland, WA, 2005.

(23) Troullier, N.; Martins, J. L. *Phys. Rev. B* **1991**, *43*, 8861.

(24) Perdew, J. P.; Burke, K.; Ernzerhof, M. *Phys. Rev. Lett.* **1996**, *77*, 3865.

(25) Bloechl, P. E.; Parrinello, M. *Phys. Rev. B* **1992**, *45*, 9413.

(26) Gilbert, B.; Huang, F.; Lin, Z.; Goodell, C.; Zhang, H.; Banfield, J. F. *Nano Lett.* **2006**, *6*, 605.

(27) Miller, J. B.; Siddiqui, H. R.; Gates, S. M.; Russell, J. N., Jr.; Yates, J. T., Jr.; Tully, J. C.; Cardillo, M. J. *J. Chem. Phys.* **1987**, *87*, 6725.

(28) King, D. A. *Surf. Sci.* **1975**, *47*, 384.

(29) Munuera, G.; Stone, F. S. *Discuss. Faraday Soc.* **1971**, *52*, 205.

(30) McHale, J. M.; Auroux, A.; Perrota, A. J.; Navrotsky, A. *Science* **1997**, *277*, 788.

(31) Gale, J. D. *General Utility Lattice Program*, version 3.0; Nanochemistry Research Institute, Curtin University of Technology: Perth, Australia, 2006.

(32) Pauling, L. *The Nature of the Chemical Bond*, 3rd ed.; Cornell University: Ithaca, NY, 1960.

(33) Zhang, H.; Penn, R. L.; Hamers, R. J.; Banfield, J. F. *J. Phys. Chem. B* **1999**, *103*, 4656.

(34) Sakaguchi, M.; Shibuki, K. *Nippon Kagaku Zasshi* **1965**, *86*, 1123.